ACKNOWLEDGEMENTS

I would like to thank my supervisor Professor H. K. D. H. Bhadeshia for welcoming me within his Phase Transformations Research Group in the Department of Materials Science and Metallurgy at the University of Cambridge and for his support during the project. I am grateful to Doctor T. Sourmail for his help, knowledge and friendship.

Thanks also to the present members of the Phase Transformation Research Group for their support and friendship.

CONTENTS

INTRODUCTION

"L'argent est le nerf de la guerre". This French phrase which emphazises the importance of the financial aspect of things could quite fairly be applied to the industrial world. Obviously, this statement is not expected to be a revelation for any of the people who read this report, neither too will it be unexpected in the last few years the environmental stakes have been emphasised as a concern relevant in the leading decisions. Besides, most of the time these two considerations lead in opposite ways because of the "cost" of environmental care.

However, in the case studied here they go in the same direction: the one of an increasing efficiency of power plants, the efficiency describing the proportion of energy fed in by burning fuel that is converted into electricity. The benefits of such an increase would be both economic and environmental, as higher efficiency would allow a decrease in the consumption of fuel, hence also a reduction in emissions of environmentally-damaging waste products (particullarly CO_2).

The major factors affecting the efficiency of steam power plants are the temperature and the pressure of the steam entering the turbines, with a predominance for the temperature since the efficiency is proportional to $(T_H-T_L)/(T_H-0)$, where T_H is the highest absolute temperature and T_L the lowest absolute temperature in the operating cycle.

Obviously changes in temperature or pressure have consequences on materials used to build boilers or turbines. That is why new materials, particularly steels, have to be designed in order to withstand extreme conditions. It is from this perspective that high-strength, high Cr ferritic creep-resistant steels have been designed.

Over the past few years, a part of the work done within the Department of Material Sciences and Metallurgy of the University of Cambridge has been to enhance the knowledge on this family of steels, particularly from the point of view of quantitative modelling.

My own work within the Phase-Transformation Research Group has been to elaborate a model dealing with the nucleation, growth and coarsening that could be applied such steels.

The first part of this report summarises general working of a fossil-fired power plant, the evolution of the ferritic creep-resistant steels and associated problems. The second part deals with the classical theory for nucleation, growth and coarsening in the solid state, and finally, the last part is dedicated to the presentation and explanation of the models that have been compiled during the four months project.

I POWER PLANTS AND STEELS

I . 1 General working of a power plant

The case of a coal-fired power plant is chosen in order to explain the functioning of an electricity generator. Nonetheless, the principles are expected to be the same for a gas-fired or nuclear power plant, at least as far as the boiler-turbine part is concerned.

Figure 1.1 is a schematic representation of a typical coal-fired power plant.

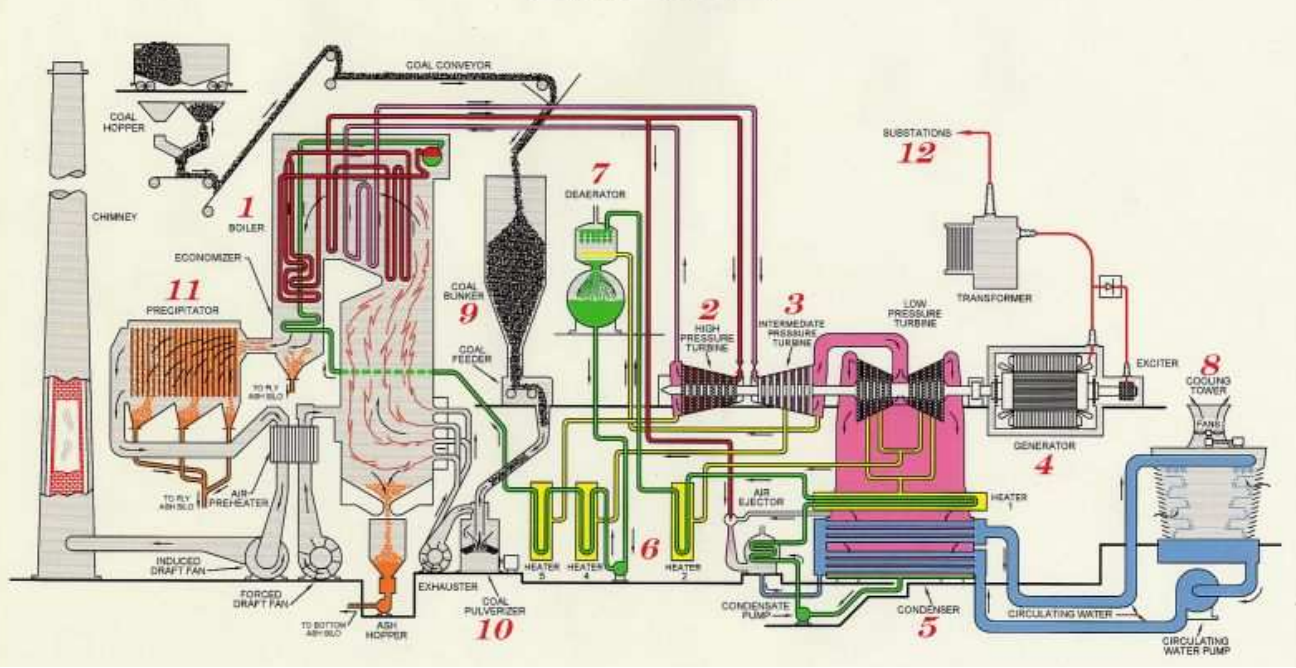

Figure 1.1: Schematic representation of the functioning of a coal-fired power plant [1].

- The fuel supply to the boiler constitutes the first stage of the process.
- The pulverized coal (pulverizer (10)) is then mixed with air and blown into the boiler for combustion.
- Millions of litres of purified water are pumped through several hundred miles of tubes inside the boiler. Heat resulting from the burning of the fuel boils this water and the steam is collected at the top of the boiler.
- Ash is collected thanks to collection system at the bottom of the boiler and, on the other hand via a precipitator (11) which allows a reduction in emissions of fly-ash into the atmosphere.
- The high-pressure steam from the boiler goes into a high pressure turbine (2), consisting of fan-type blades attached to a shaft against which the steam flows causing the shaft to turn. The steam coming out from this turbine with both temperature and pressure reduced is then sent to be reheated (either

directly into the boiler itself or into a reheater) and passes into an intermediate pressure turbine (3). The steam that exits this second turbine goes into a low pressure turbine and is finally admitted to the condenser (5) where it is cooled by circulating cold water. Then the obtained water can restart the cycle.

- The motion of the turbines is transmitted to a generator to produce electricity.

Figure 1.2: Turbine-generator set. In the foreground is the high pressure turbine, follow the intermediate and low pressure turbines, and eventually in background is the generator [1].

Stage	*Entry pressure and temperature*		*Exit pressure and temperature*	
High pressure	16 MPa	565 °C	4 MPa	420 °C
Intermediate pressure	4 MPa	565 °C	0.6 MPa	250 °C
Low pressure	0.6 MPa	250 °C	0.1 MPa	100 °C

Table 1.1: Example of steam conditions in a turbine-generator set [2].

The typical efficiency of such a power plant approches 40%. Increasing reasonably both temperature and pressure of the steam, efficiency could then become closer to 45%.

However, the extreme conditions associated with the greater temperatures and pressures require new materials, hence the development of the high-strength martensitic creep-resistant steels.

I . 2 The steels

The choice has been made to talk only about the martensitic creep-resistant steels. Nevertheless, it is important to notice that other kinds of steels and, more generally, of materials are likely to be found in the different parts forming the huge edifice that constitutes a power plant (austenitic stainless steels, Ni-base alloys, ceramics, ...).

As implied in the previous part, an increase of temperature and pressure of the steam conveyed through the boiler and entering the turbines (especially the high pressure turbine) requires materials with specific properties. Among the most important, a high strength and corrosion resistance together with good fabricability and weldability.

To give some figures, the typical tolerable creep strain rate for a power plant steel is about $3.10^{-11}s^{-1}$, which represents only 2% elongation over the 30 years [2]. Furthermore, the material must be able to support a stress of 100 MPa at service temperature over a time period of 10^5 h without rupture.

It is in order to overcome that challenge that have been developed the 9-12 wt.% Cr steels with a martensitic structure.

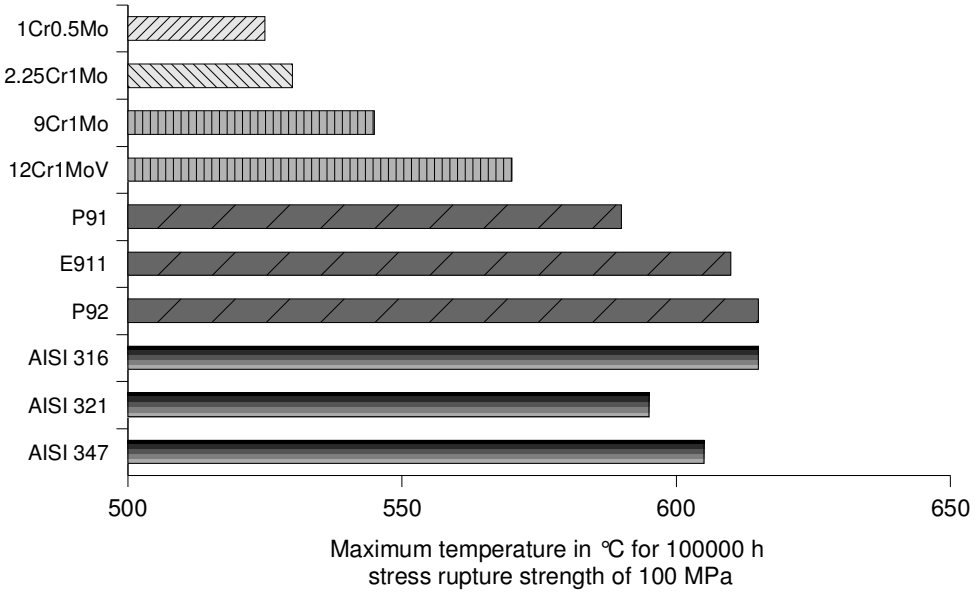

Figure 1.3: Maximum temperature for the application of various power plant steels based on a 10^5 h stress rupture strength of 100 MPa [3].

Figure 1.3 shows results after a classical long-term creep-resistance test for a few steels. The stress rupture strengths of the later high Cr martensitic steels (P91, E911 and P92) match the ones of austenitic stainless steels (AISI 316, AISI 321 and AISI 347).

Besides, the martensitic structure brings other advantages in comparison with the austenitics: lower coefficients of thermal expansion and better thermal conductivities, both enhancing the thermal fatigue resistance.

The reasons of the choice of each alloying element added to a tempered martensitic

microstructure steel has been clearly summed up by Abe et al [4] in the *Alloy design philosophy for high Cr ferritic steels.*

- The Chromium allows the steel to be oxidation resistant, nonetheless, too high a concentration of Cr stimulates the formation of δ-ferrite generally regarded as harmful for the creep rupture strength (Fig 1.4).

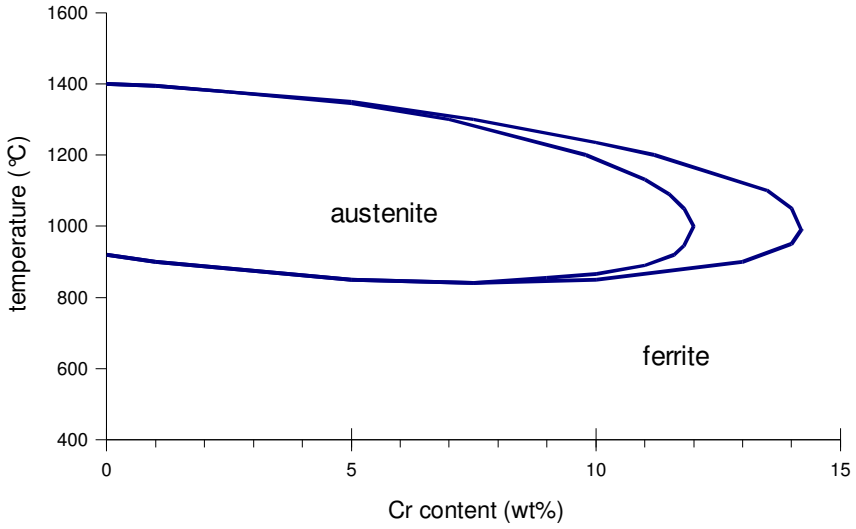

Figure 1.4: Constitutional diagram for Fe-Cr alloys.

- The optimal concentration in Cr is 9 wt.% so that the formation of δ-ferrite be avoided and the oxidation resistance remain acceptable. However, this concentration can reach 12 wt.% (or even more) thanks to additions of austenite stabilising elements such as Ni, Cu or Co.

- The silicon acts in the same way that Cr with an improvement of the corrosion resistance until 0.5 wt.% and a risk of formation of δ-ferrite beyond this concentration.

- Optimising the amounts of C, N and B, the long-term creep rupture strength of the steel can also be enhanced.

- Finally, the development of 9-12 wt.% Cr steels has known a real growth thanks to the additions of Nb and V, followed later by W (Fig 1.5).

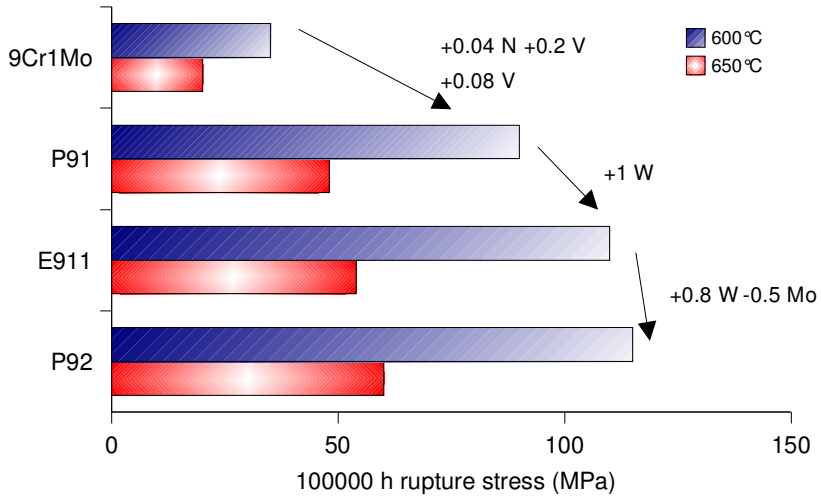

Figure 1.5: Development of 9 wt.% Cr steels [3].

We could wonder why those elements are so important for the long-term creep resistance of the steels in interest. The answer would be then that Nb, V and W are strong factors acting in the strengthening mechanisms by combining with C and N and forming fine carbide and nitride precipitates, and to a less extent carbonitride precipitates.
Then, during the early stages of the creep deformation, those precipitates are expected to interact with the moving dislocations and therefore to slow down significantly the creep rate of the alloyed steel.

- Others additions have also been attempted like for instance, B, Pd or Y with varied results more or less promising [4].

Unfortunately and despite the efforts to overcome them, there are still problems to be solved, hence the need of such a search.

I . 3 Some problems

The experience shows that drop in the creep resistance, and therefore in the capacity to withstand the rupture, of many power plant steels during service at high temperature is mainly due to an embrittlement at the grain boundaries.

As stated by Bhadeshia [1], the martensitic microstructure of the 9-12 wt.% Cr power plant steels is the result of a disciplined motion of atoms. However this transformation cannot fully occur in the vicinity of the grain boundary. The consequence is the persistence of vestiges of the austenite grain boundary, called prior austenite grain boundary (PAGB), which form preferential sites for impurity

segregation and/or for carbide precipitation and coarsening, both detrimental to creep.

The case of the 9Cr1MoVNb steel (ASME T91) has been studied in depth by Kimura et al [5] who have correlated on the one hand a preferential precipitation, growth and coarsening of a kind of nitride precipitate (Z-phase) with a recovery occurring especially in the vicinity of the PAGB (during long-term creep test) and, on the other hand, this heterogeneous recovery with the degradation of the long-term creep resistance of the steel (Fig 1.6 & 1.7). Other precipitates such as $M_{23}C_6$ or the Laves phases (Fe_2(W,Mo,Nb)) are suspected to have similar effects on the long-term creep resistance.

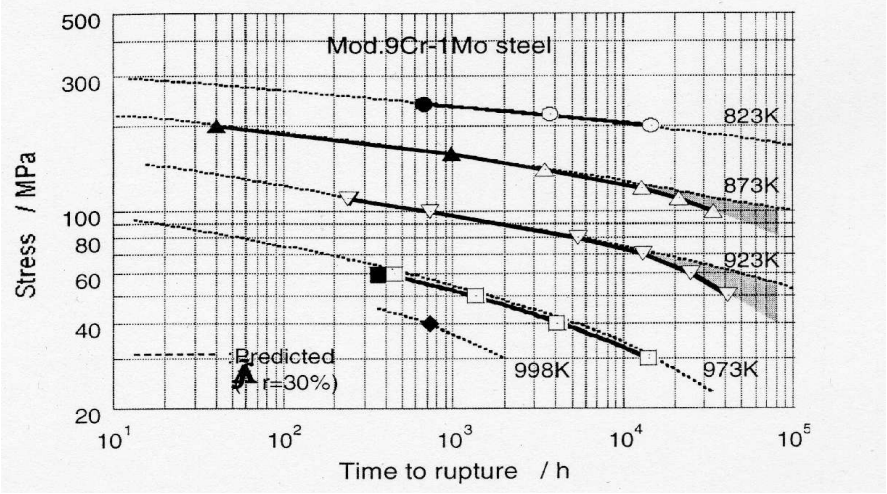

Figure 1.6: Degradation in creep rupture strength at long time [5].

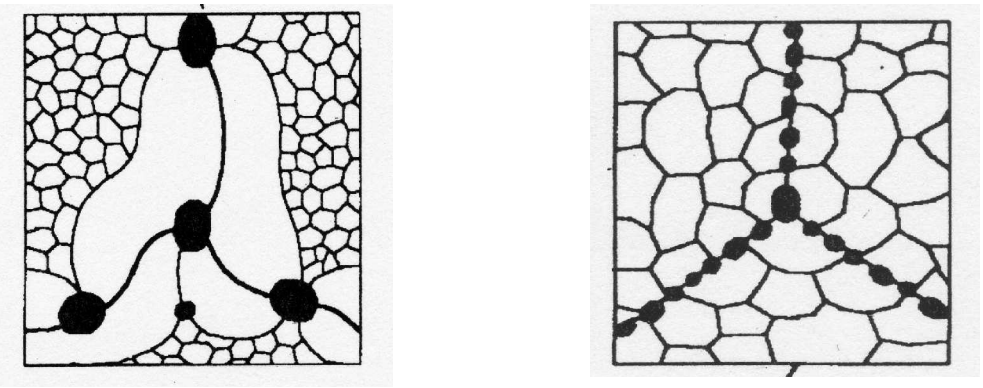

Figure 1.7: Illustration of the preferential recovery in the vicinity of the PAGB in the case of a long-term creep test (at the left). The picture at the right is for a short-term creep test [5].

Considering these studies, the problems of embrittlement seem quite clearly to be linked to the behaviour of the precipitates at the grain boundary.

The following part describes the theorical tools necessary to deal with the precipitation phenomenon, that is the nucleation, growth and coarsening stages.

II THEORY FOR NUCLEATION, GROWTH AND COARSENING OF PRECIPITATES IN THE SOLID STATE

The aim of this chapter is to summarise the theory on the formation and evolution of the precipitates in the solid state, as used within the models presented in the third part of this report.

II . 1 Nucleation

This phenomenon has to be understood as a balance between two energies: the free energy available from the driving force and the energy consumed in creating a new interface between parent and product phases. Once the rate of change of free energy becomes negative, then an embryo can grow.

Two kinds of nucleation can occur in a material: homogeneous and heterogeneous nucleation. In practice, homogeneous nucleation is extremely rare (only two cases are known in the solid state: Cu with 1-3 wt.% Co that can be heat treated to precipitate Co homogeneously and Ni_3Al in Ni superalloys), whereas the heterogeneous one is much more common.

However it is traditional to start with the simplest of the two, that is the homogeneous nucleation to explain the bases of the theory.

II . 1 . a Homogeneous nucleation

We have made the assumption for both types of nucleation that the new product phase appears as spherical particles.
Considering the formation of a nucleus of θ in a matrix α, the change in Gibbs energy is:

$$\Delta G = \frac{4\pi r^3}{3}\Delta G_v + 4\pi r^2 \sigma_{\alpha\theta} \qquad (2.1)$$

where r is the radius of the nucleus, ΔG_v is the Gibbs energy change per unit volume of embryo and $\sigma_{\alpha\theta}$ is the interfacial energy per unit area.

Here, the possible elastic energy due to the volume changes between parent and product phases has been neglected.

Differentiating (2.1), it can be found the critical radius r^* and the activation energy G^* at which the rate of change of free energy turns negative (Fig 2.1).

$$r^* = \frac{-2\sigma_{\alpha\theta}}{\Delta G_v} \quad \text{and} \quad G^* = \frac{16\pi}{3}\frac{\sigma_{\alpha\theta}^3}{\Delta G_v^2} \qquad (2.2)$$

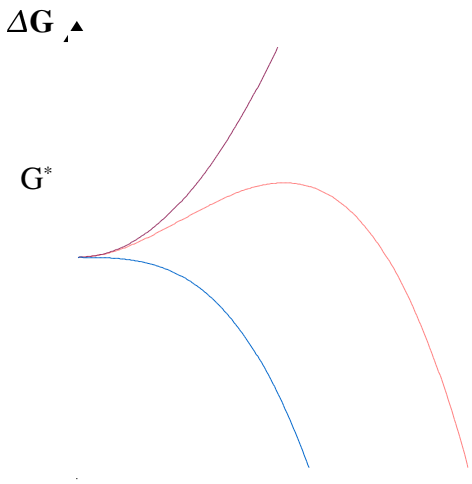

Figure 2.1: Variation of the Gibbs energy change with the radius of a nucleus for an homogeneous nucleation.

It becomes then possible to estimate the nucleation rate I.

$$I = N^* f \qquad (2.3)$$

where N^* is the number density (or population) of embryos of the critical size and f is the rate at which such embryos are formed. N^* and f follow the Boltzmann statistics:

$$N^* = N \exp\left(-\frac{G^*}{RT}\right) \quad \text{and} \quad f = \nu \exp\left(-\frac{Q}{RT}\right) \qquad (2.4)$$

where N is the number density of sites (for homogeneous nucleation N is the number of atoms per unit volume), ν an attempt frequency, Q the activation energy for tranfert of atoms across the matrix-precipitate interface, R the gas constant and T the absolute temperature.

Then replacing in (2.3):

$$I = N \nu \exp\left(-\frac{G^* + Q}{RT}\right) \qquad (2.5)$$

- The unit of I is number of nuclei.m^{-3}.s^{-1}.
- ν is often taken as being $\frac{kT}{h}$ where h is the Plank constant.

II . 1 . b Heterogeneous nucleation

Several sorts of heterogeneous nucleation are likely to take place in the same material, most of the time at different scales, for instance, at dislocations, on grain corners or on boundaries.

Consider the example of the grain boundary nucleation (Fig 2.2). The formation of a nucleus is helped because it suppresses a high energy defect.

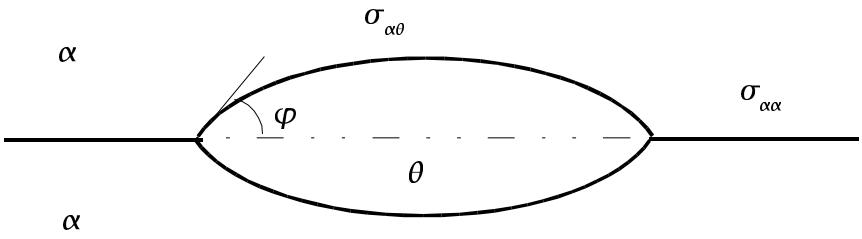

Figure 2.2: Illustration of the nucleation on a grain boundary [6].

The expression of the critical radius remains the same as in homogeneous nucleation. The activation energy changes to [6]:

$$G_{GB}^{*} = \frac{4}{27} \frac{\left(\eta_{\alpha\,0}\,\sigma_{\alpha\,0} - \eta_{\alpha\,\alpha}\,\sigma_{\alpha\,\alpha}\right)^{3}}{\eta_{0}^{2}\,\Delta G_{v}^{2}} \qquad (2.6)$$

where $\sigma_{\alpha\alpha}$ and $\sigma_{\alpha\theta}$ are respectively the interfacial energies for the grain boundary and for the interface precipitate-matrix. η_{θ}, $\eta_{\alpha\theta}$, $\eta_{\alpha\alpha}$ are shape factors.

$$\begin{aligned} \eta_{\alpha\,\alpha} &= \pi \sin^{2}(\varphi) \\ \eta_{\alpha\,0} &= 4\,\pi\left(1 - \cos(\varphi)\right) \\ \eta_{0} &= 2\,\pi\,\frac{\left(2 - 3\cos(\varphi) + \cos^{2}(\varphi)\right)}{3} \end{aligned} \qquad (2.7)$$

And I_{GB} is given by:

$$I_{GB} = N_{GB}\,\nu\,\exp\left(-\frac{G_{GB}^{*} + Q}{RT}\right) \qquad (2.8)$$

where N_{GB} is the number density of sites on the grain boundary ($<< N$).

II . 2 Growth

II . 2 . a Introduction

It is important to notice that all the present work has been performed for a binary system (e.g., Fe-C). Theories involving multicomponent systems exist ([7], [8], [9], [10]) and could be applied to it later.

It is assumed that the growth of precipitates is diffusion-controlled (as opposed to interface-controlled), so the majority of the free energy is dissipated in the diffusion of solute ahead of the interface (Fig 2.3).

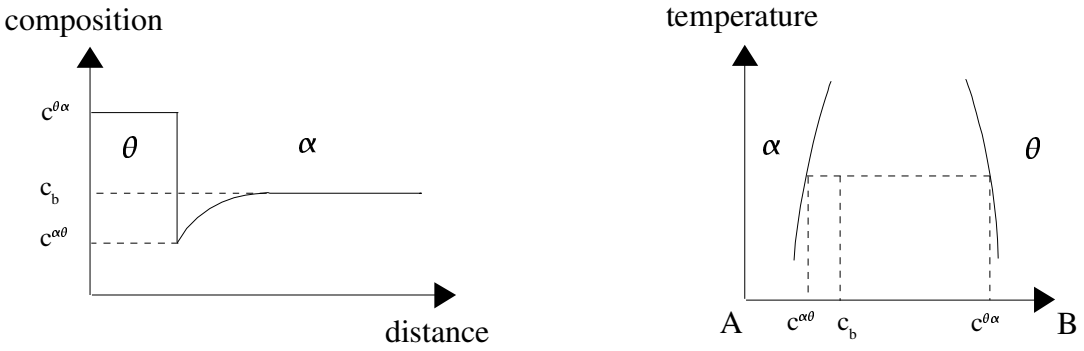

Figure 2.3: Schematic illustration of the solute concentration profile at the interface between the precipitate α and the matrix θ, and the binary phase diagram giving the compositions at this interface. $c^{\theta\alpha}$ is the concentration of solute in the precipitate in equilibrium with α, similarly $c^{\alpha\theta}$ is the concentration of solute in the matrix in equilibrium with θ. c_b is the bulk concentration.

We begin with the simple Zener model [11] for the growth of a planar interface with a constant far-field concentration (c_b).

II . 2 . b The Zener model

In this model it is assumed that gradient of concentration is constant as illustrated below (Fig 2.4).

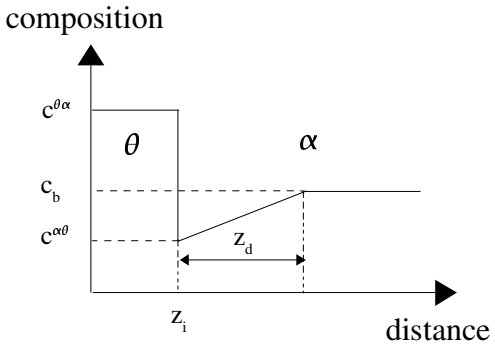

Figure 2.4: Solute concentration profile with the constant concentration gradient approximation.

By Fick's law for diffusion, the flux of solute arriving at the interface is:

$$J_{z=z_i} = -D\frac{\partial c}{\partial z}\Big|_{z=z_i} \qquad (2.9)$$

where z_i is the position of the interface, D is the diffusion coefficient of the solute in the matrix and c the concentration of solute.

For a constant gradient, (2.9) becomes:

$$J_{z=z_i} = -D\frac{c_b - c^{\alpha\theta}}{z_d} \qquad (2.10)$$

where z_d is a diffusion distance.

This flux must equal the rate at which the solute is added to the precipitate:

$$\in J_{z=z_i} \in = \psi\left(c^{\theta\alpha} - c^{\alpha\theta}\right) \qquad (2.11)$$

where ψ is the interface velocity.

The relationship between z_i and z_d is given by mass conservation:

$$\frac{1}{2}z_d\left(c_b - c^{\alpha\theta}\right) = z_i\left(c^{\theta\alpha} - c_b\right) \qquad (2.12)$$

Then combining (2.11) and (2.12) and introducing the supersaturation (dimensionless) $\Omega=(c_b-c^{\alpha\theta})/(c^{\theta\alpha}-c^{\alpha\theta})$, we obtain:

$$\psi = \frac{dz_i}{dt} = \frac{1}{2z_i} D\,\Omega\,\frac{c_b - c^{\alpha\theta}}{c^{\theta\alpha} - c_b} \qquad (2.13)$$

Finally, assuming that $\left(c^{\theta\alpha} - c_b\right) \simeq \left(c^{\theta\alpha} - c^{\alpha\theta}\right)$:

$$\psi = \frac{dz_i}{dt} = \frac{1}{2z_i} D\,\Omega^2 \qquad (2.14)$$

Integration gives:

$$z_i = \Omega\sqrt{Dt} \quad \text{and} \quad \psi = \frac{\Omega\sqrt{D}}{2\sqrt{t}} \qquad (2.15)$$

which is the classical parabolic law for diffusion-controlled growth in a binary system.

II . 2 . c A more rigorous approach

According to the review by Christian [6], for one-, two- or three-dimensional geometries, the relation given the position of the interface is:

$$r_i = \gamma\sqrt{Dt} \qquad (2.16)$$

where γ is the solution of:

$$\gamma^j = 2\,\Omega\,\frac{\exp\left(-\frac{\gamma^2}{4}\right)}{\varphi_j(\gamma)} \qquad (2.17)$$

where Ω is the supersaturation, j is 1, 2 or 3 depending on the geometry of the problem: planar, cylindrical or spherical, and $\varphi_j(\gamma)$ is defined as:

$$\varphi_j(\gamma) = \int_{\gamma}^{\infty} u^{1-j} \exp\left(-\frac{\gamma^2}{4}\right) du \qquad (2.18)$$

These relatively complicated expressions can be simplified using asymptotic expansions of $\varphi_j(\gamma)$ in the cases in which Ω is close to 0 (and it will be the case in practical for us), for the planar and spherical geometries, to obtain:

$$\gamma^{planar} = \frac{2}{\sqrt{\pi}}\Omega \quad \text{and} \quad \psi = \frac{\Omega\sqrt{D}}{\sqrt{\pi\,t}} \qquad (2.19)$$

$$\gamma^{spherical} = \sqrt{2\,\Omega} \quad \text{and} \quad \psi = \frac{\sqrt{\Omega\, D}}{\sqrt{2\,t}} \qquad (2.20)$$

The relations (2.19) and (2.20) are widely used within the models of the third part to characterize the behaviour of the precipitates. Most of the time they are associated with the capillarity effect.

II . 2 . d The capillarity effect

Also known as the Gibbs-Thomson effect, capillarity arises from the influence of interfacial energy which must then been taken into account.
From figure 2.5, it can be seen that there is a modification of equilibrium.

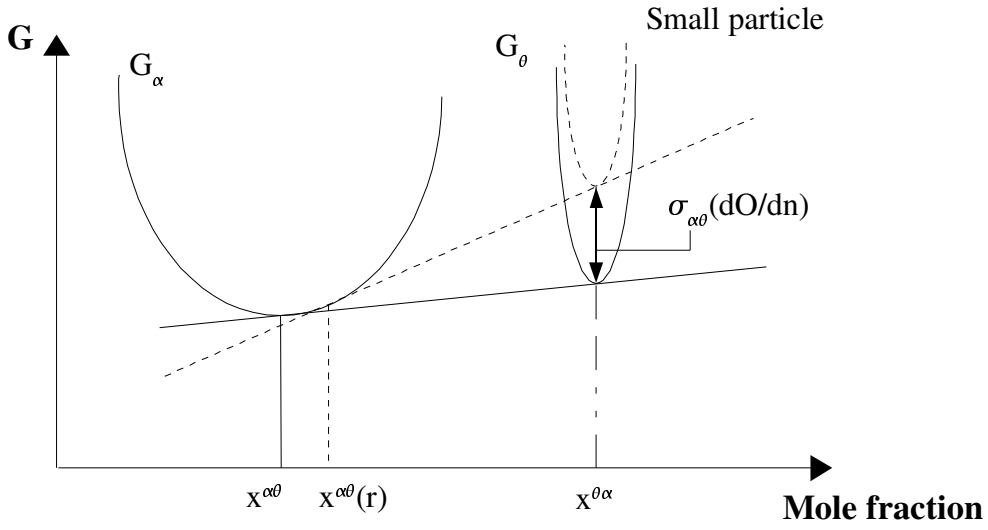

Figure 2.5: Illustration of the Gibbs energy and composition changes due to the capillarity effect. $x^{\theta\alpha}$ is the mole fraction of solute in θ in equilibrium with α, $x^{\alpha\theta}$ the mole fraction of solute in α in equilibrium with θ, and $x^{\alpha\theta}(r)$ is the corrected value for a precipitate with a curvature radius of r.

The increase in Gibbs energy due to the expanding area is given by (Fig 2.5) [6]:

$$G_\theta(r) - G_\theta = \sigma_{\alpha\theta}\frac{dO}{dn} \qquad (2.21)$$

where $\sigma_{\alpha\theta}$ is the interfacial energy for the matrix-precipitate interface and dO/dn is the increase of interface area when a mole of component is transfered to the precipitate. dO/dn becomes $2V_m^\theta / r$ where V_m^θ is the molar volume of the precipitate and r the radius of curvature of the particle, in the case of spherical geometry.

The modified value of $x^{\alpha\theta}$ is given by the Gibbs Thomson equation which can be written as being:

$$x^{\alpha\theta}(r) = x^{\alpha\theta} \exp\left(\frac{2 V_m^{\theta} \sigma_{\alpha\theta}}{r} \frac{1}{RT\left(x^{\theta\alpha} - x^{\alpha\theta}\right)} \right) \qquad (2.22)$$

The capillarity effect is also the origin of coarsening phenomena.

II . 3 Coarsening

To some extent, the coarsening stage can be seen as a part of the growth, since it is the phase during which the small particles dissolve at the expense of the larger ones in order to reduce the total surface area.

Typical coarsening behaviour is summurised in the figure 2.6 with, at the same time, a decrease of the number of particles and an increase of their average size.

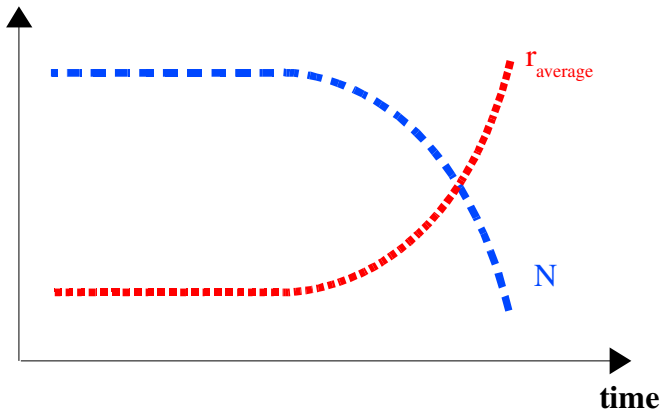

Figure 2.6: Evolution of the number of particles N and of the mean size $r_{average}$ of those particles during the coarsening stage.

The process leading to coarsening is as follows:

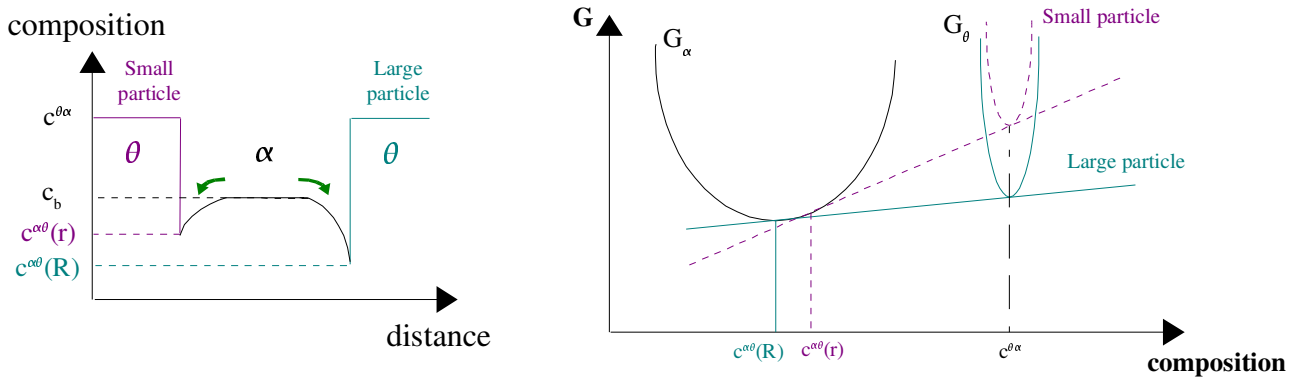

After nucleation and beginning of the growth, the situation is that several distribution (N, radius) coexist and all the precipitates grow pumping solute from the matrix.

Since the growth continues, the bulk concentration decreases because of the drain of solute by the growing particles. (r and R ↗)

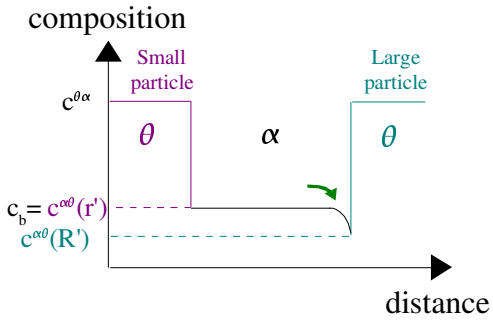

Small particles stop growing, whereas the growth of the larger ones goes on. c_b still decreases. ($r'>r$ and $R'>R$)

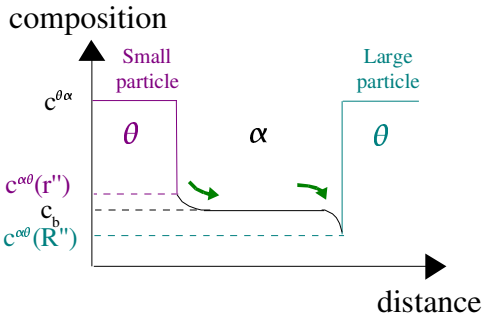

Small particles start dissolving « at the expense » of the large ones until their whole disappearance.

($r'' < r'$ and $R'' > R'$)

As seen in the paragraph I . 3, coarsening and particularly coarsening within the grain boundary is often considered as harmful in the quest to reach the best creep resistance of the steel. Besides, the factors limiting its spread remain relatively bad known.

III THE MODELS

III . 1 Introduction

Within a scientific field such as metallurgy which has traditionally been dependant on experiments, computer modelling could be seen as a kind of mini revolution in the sense that the metallurgist swaps his fireproofed gloves for the keyboard of a computer.

The aim in general is not to replace experiments but more, through models, to make material and process design more rational. For instance, some of them are able starting from inputs like the temperature, the composition of the steel, etc..., to predict the evolution of a mechanical property such as the creep rupture strength [2] as a function of the concentration in a selected element. This kind of model giving predictions on the behaviour of the material can make alloy design considerably easier.

Here, the emphasis has been placed on the modelling of the evolution of precipitates in the solid state during exposure to a high temperature. Two different models have been created using the programming language FORTRAN.

The first program is focused particularly on the coarsening stage whereas the second one, more thorough, deals with the entire evolution of the precipitates from the nucleation to the « end » of the coarsening.

III . 2 First model

III . 2 . a Presentation

As said above, this first program is about the coarsening stage, that is to say the phenomenon in which little particles disappear and larger ones become bigger. In this case the large particles are represented by a single « particle » with an infinite radius of curvature and symbolising the grain boundary, whereas the little precipitates have a finite initial radius r_0, and are arranged randomly within the material. The number density N of those particles is linked to the bulk composition of solute in the material c_{bulk} via the matter conservation relation (3.1):

$$N = \frac{c_{bulk} - c^{\alpha\theta}(r_0)}{c^{\theta\alpha}} \frac{1}{\frac{4}{3}\pi r_0^3} \qquad (3.1)$$

where variables are as explained below.

The material is divided virtually in slices (Fig 3.1) for the purposes of computation (III . 2 . b and c), and within those slices the precipitates are assumed as being in equilibrium with the surrouding matrix. c_b, the average concentration in solute in the slices is initially taken equal to $c^{\alpha\theta}(r_i)$, that is the concentration in solute in the matrix α in equilibrium with the precipitate θ corrected and accounting

for the Gibbs-Thomson effect. Since the interface matrix-precipitate at the grain boundary is assumed to be plane ($r=\infty$), the concentration in solute in equilibrium with the precipitate at this interface is given by the value without the capillarity correction.

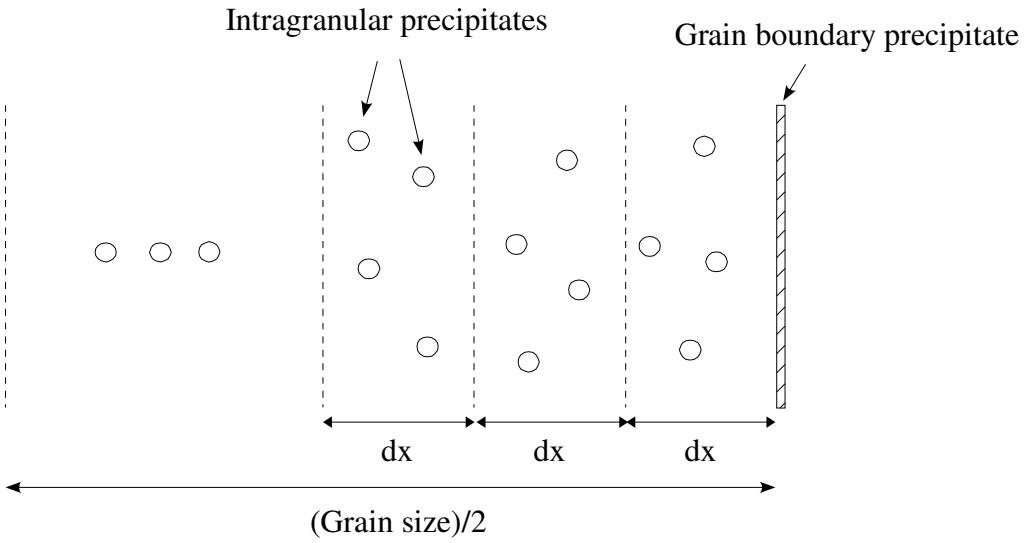

Figure 3.1: Illustration of the situation at the onset of the program.

For this model that involves diffusion between particles has been applied the finite difference method. An explanation of that method follows.

III . 2 . b The finite difference method

In order to use the Fick's laws for diffusion and given that computers have a finite amount of memory, it is necessary to discretize space and time in these equations.

$$J = -D\frac{\partial c}{\partial x} \qquad (3.2)$$

$$\frac{\partial c}{\partial t} = D\frac{\partial^2 c}{\partial x^2} \qquad (3.3)$$

The finite difference approximation [13] allows this discretization. Then, instead of solving the equations for $c(x,t)$ with x and t continuous, they are solved for $c_{i,j}=c(x_i,t_j)$ where $x_i=i\delta x$ and $t=_j j\delta t$ (Fig 3.2).

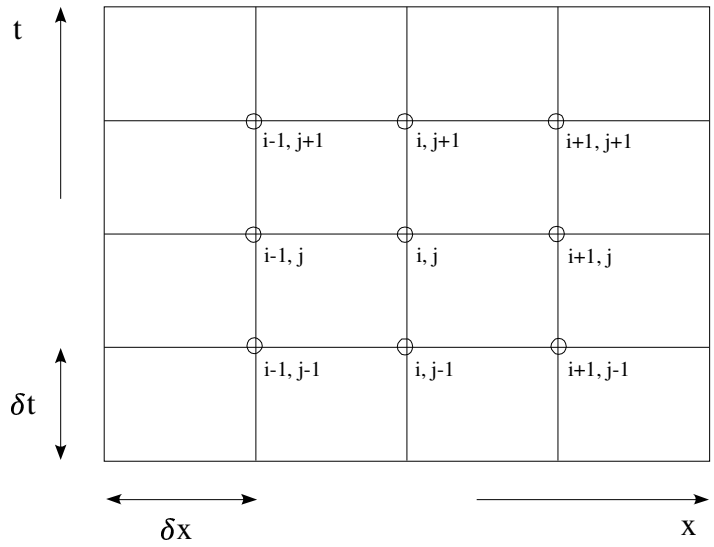

Figure 3.2: Grid for the finite difference approximation. The point labelled *i, j* corresponds to $(x, t)=(x_i, t_j)$.

The derivatives of *c* are approximated in terms of the values of *c* at grid points.

$$\frac{\partial c}{\partial x} = \lim_{\Delta x \to 0} \frac{\Delta c}{\Delta x} \qquad (3.4)$$

the derivative evaluated at the grid point (x_i,t_j) $(=(x,t))$ is approximated as:

$$\frac{\partial c}{\partial x}\Big|_{x_i, t_j} \approx \frac{c_{i+1,j} - c_{i,j}}{x_{i+1} - x_i} = \frac{c_{i+1,j} - c_{i,j}}{\delta x} \quad \text{(Forward difference)} \qquad (3.5)$$

$$\frac{\partial c}{\partial x}\Big|_{x_i, t_j} \approx \frac{c_{i,j} - c_{i-1,j}}{x_i - x_{i-1}} = \frac{c_{i,j} - c_{i-1,j}}{\delta x} \quad \text{(Backward difference)} \qquad (3.6)$$

$$\frac{\partial c}{\partial x}\Big|_{x_i, t_j} \approx \frac{c_{i+1,j} - c_{i-1,j}}{x_{i+1} - x_{i-1}} = \frac{c_{i+1,j} - c_{i-1,j}}{2\delta x} \quad \text{(Central difference)} \qquad (3.7)$$

Similarly, the second derivative at this same grid point, may be approximated by using:

$$\frac{\partial^2 c}{\partial x^2} = \lim_{\Delta x \to 0} \frac{\Delta\left(\frac{\partial c}{\partial x}\right)}{\Delta x} \qquad (3.8)$$

At this stage the more common and useful approach is to consider fictitious points with coordinates: $x_{i+1/2}$, $x_{i-1/2}$. Then using central difference approximations evaluated at these points, we obtain the following relation:

$$\frac{\partial^2 c}{\partial x^2}\Big|_{x_i,t_j} \approx \frac{\frac{\partial c}{\partial x}\Big|_{x_{i+\frac{1}{2}},t_j} - \frac{\partial c}{\partial x}\Big|_{x_{i-\frac{1}{2}},t_j}}{x_{i+\frac{1}{2}} - x_{i-\frac{1}{2}}} = \frac{c_{i+1,j} - 2c_{i,j} + c_{i-1,j}}{(\delta x)^2} \qquad (3.9)$$

Following the same procedure, we can apply this approximation to the time derivative:

$$\frac{\partial c}{\partial t}\Big|_{x_i,t_j} \approx \frac{c_{i,j+1} - c_{i,j}}{t_{i+1} - t_i} = \frac{c_{i,j+1} - c_{i,j}}{\delta t} \qquad (3.10)$$

Then using (3.9) and (3.10) in (3.3), the equation (3.11) is gotten and gives an expression of c at t_{j+1} as a function of c at t_j.

$$c_{i,j+1} = c_{i,j} + \frac{D\delta t}{(\delta x)^2}\left(c_{i+1,j} - 2c_{i,j} + c_{i-1,j}\right) \qquad (3.11)$$

This expression is dependent of the choice of δx and δt. The closer they are to zero, the less important is the truncation error. This kind of scheme is called *consistent*. However, the *consistence* is not all given that the solution of the discretized equation (3.11) must approach the exact solution of (3.3) in the limit that $\delta x \to 0$ and $\delta t \to 0$. This aspect, called *convergence,* is intimately related to the *stability* of the numerical scheme in the case of linear equations such as the diffusion equations (a scheme is called *stable* if it does not magnify errors that arise during the calculation). It can be shown [13] that in this case, the scheme is only stable when:

$$\frac{D\delta t}{(\delta x)^2} \leqslant \frac{1}{2} \qquad (3.12)$$

In practice, the aim is often to find the good compromise between an « acceptable » error and a reasonable time of calculation.

III . 2 . c Working of the program

There are two phenomena occurring at the same time in the material. On the one hand, the diffusion of the solute between adjacent « slices », on the other hand, the dissolution of precipitates. They are closely linked in the sense that the matter coming from dissolution of the particles provides the matrix with solute which is then conveyed through the slices and as far as the grain boundary thanks to diffusion.

The detailed functioning is as follows:

- The whole process is initialised by the gradient of concentration in solute existing at the interface matrix (first slice)-grain boundary (Fig 3.1). This situation leads to diffusion through this interface and therefore to an increase in the thickness of the grain boundary.

- Increase in the thickness of the grain boundary means a drain of solute from its vicinity, symbolised by the first slice, and then a decrease of the average concentration in solute in this part (initially equal to $c^{\alpha\theta}(r_0)$ where r_0 is the initial mean radius of the precipitates).

- At this stage, the average concentration in solute in the matrix in the first slice is lower than the value of $c^{\alpha\theta}(r_0)$ at the interface (precipitates of the first slice)-matrix, entailing therefore the beginning of the dissolution of these particles.
  Dissolution is calculated using the expression (2.20) of the interface velocity modified to be as a function of the radius of the particles:

$$\psi = \frac{\Omega D}{r} \qquad (3.13)$$

  where Ω is the supersaturation given by $(c_b\text{-}c^{\alpha\theta}(r))/(c^{0\alpha}\text{-}c^{\alpha\theta}(r))$.

  After dissolution, the new mean radius of the particles is:

$$r_n = r_f + \psi\, dt \qquad (3.14)$$

  where r_n and r_f are the radii after and before dissolution respectively and dt is the step time.

  The global amount of matter lost by the particles of the slice is:

$$dV = N V_s 4\pi r_f^2 \psi\, dt \qquad (3.15)$$

  where N is the number density of particles and V_s the volume of the slice.

  Finally, a new average composition in solute in the slice is calculated to take into account this contribution of solute coming from the dissolution:

$$c_{bn} = c_{bf} + \frac{dV}{V_s}\left(c^{0\alpha} - c^{\alpha 0}(r)\right) \qquad (3.16)$$

  where c_{bn} and c_{bf} are respectively the new and the former mean composition in solute of the slice.

- Dissolution of particles spreads naturally to the other slices of the material given that the solute concentration profile is calculated at each step of time dt thanks to the finite difference method and more precisely, using the relation (3.11).

- The situation within the last slice is particular in the sense that the concentration in solute in it can not be calculated with a real central difference. The solution is to consider the existence of a fictitious slice beyond the last one following the same behaviour as the one just before (reflexion). The relation (3.11) becomes:

$$c_{imax\ ,\ j+1} = c_{imax\ ,\ j} + \frac{D\,\delta\,t}{\left(\delta\,x\right)^2} 2\left(c_{imax-1,\,j} - c_{imax\ ,\ j}\right) \qquad (3.17)$$

where *imax* symbolises the last slice.

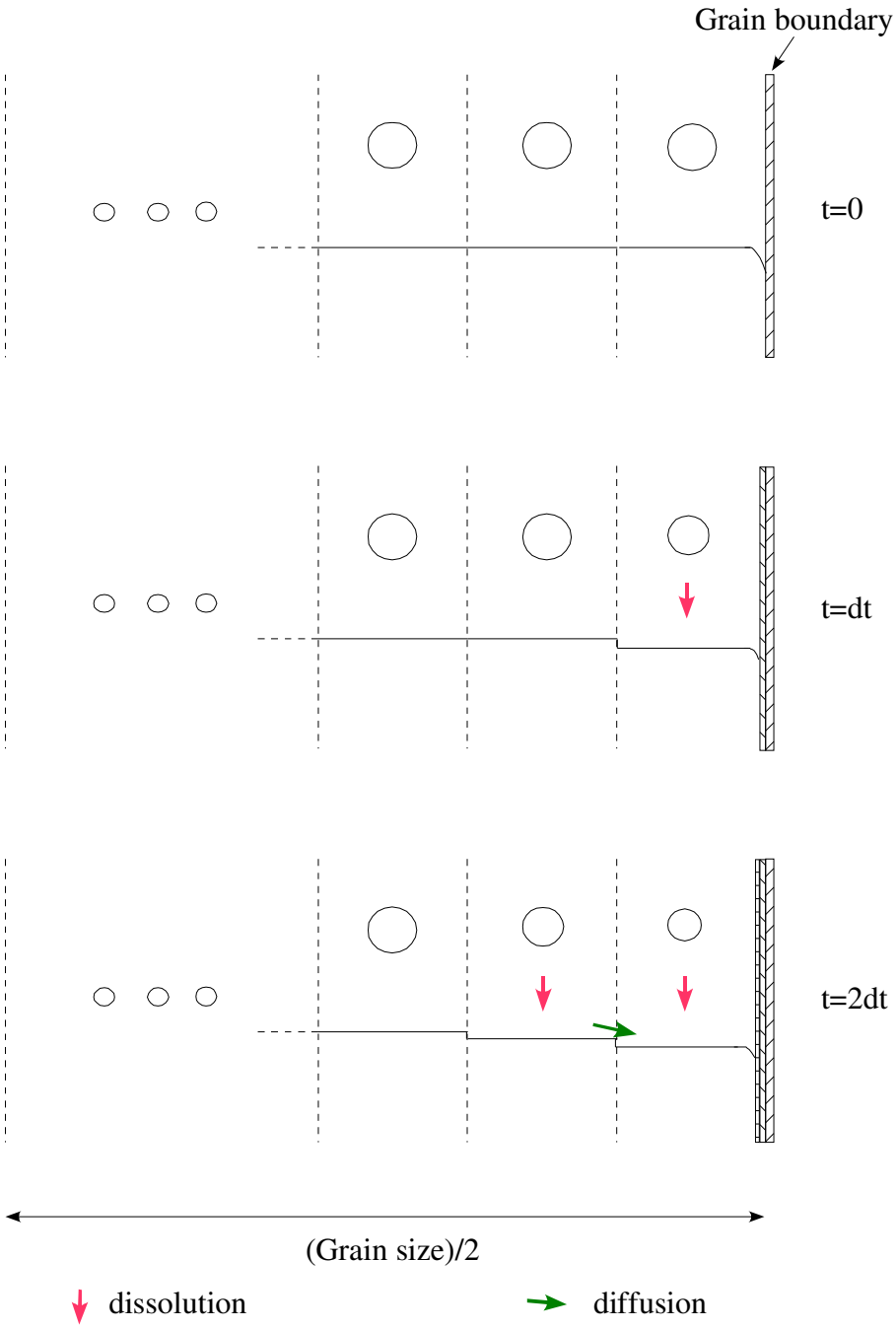

Figure 3.3: Early stages of the model.

III . 2 . d Results and discussion

A first result of this model takes the shape of a curve on which can be seen the evolution of the thickness of the grain boundary as a function of the time (or square root of time) (Fig 3.4).

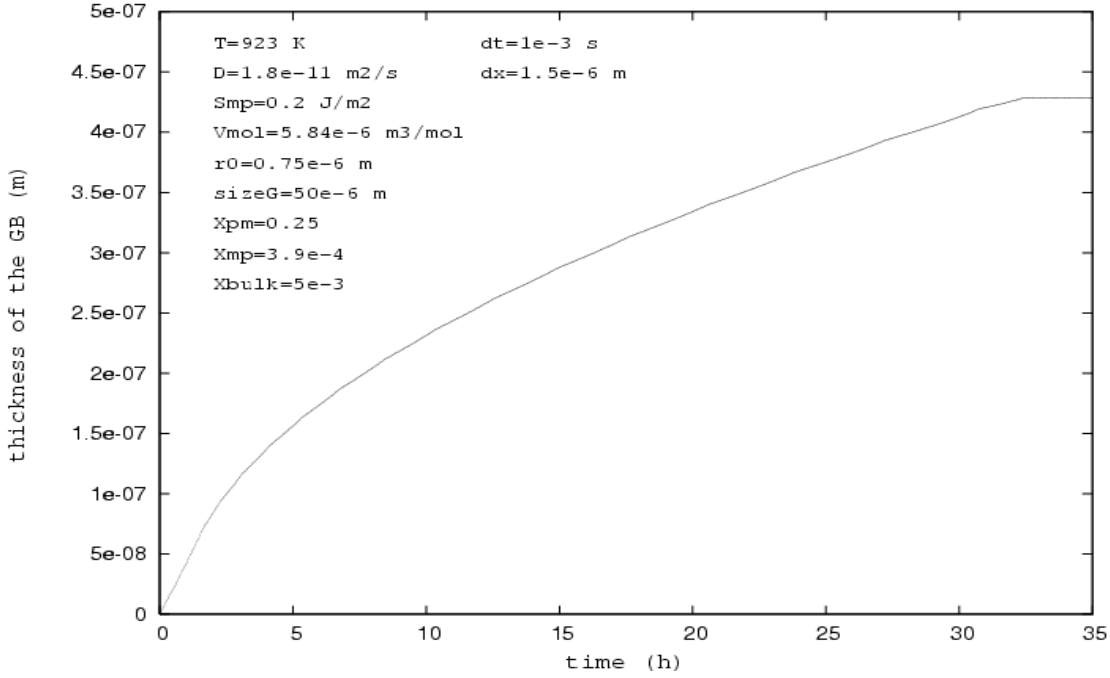

(a)

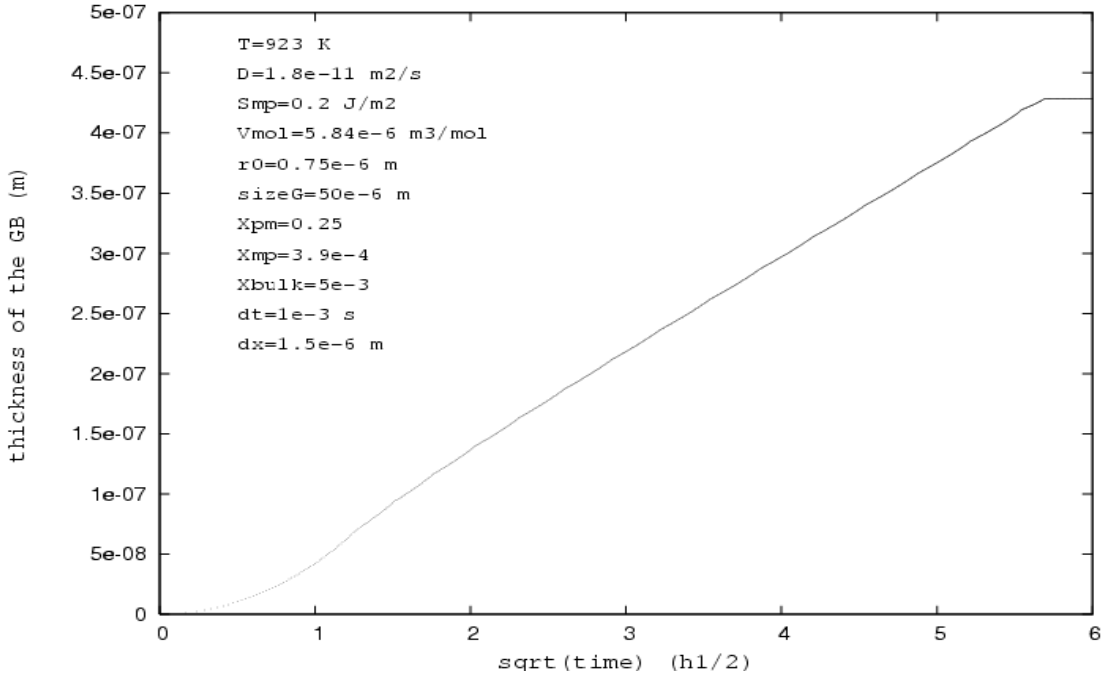

(b)

Figure 3.4: Thickness of the grain boundary precipitate as a function of time (a) and as a function of the square root of time (b).

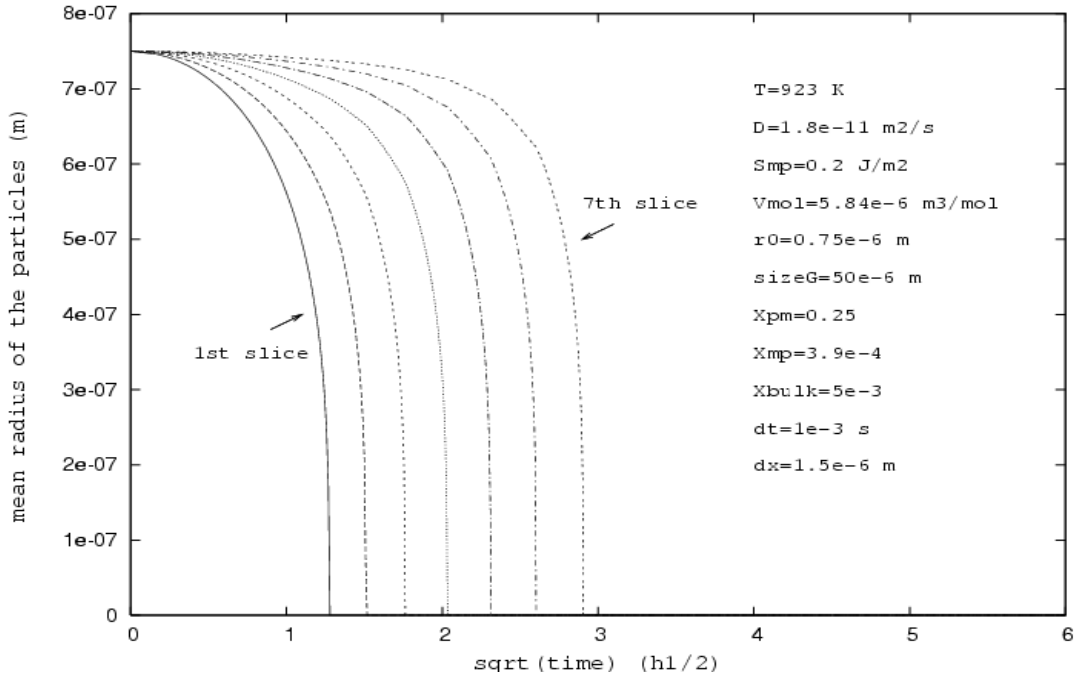

Figure 3.5: Evolution of the size of the particles in each slice as a function of the square root of time.

Figure 3.5 gives in parallel with the evolution of grain boundary thickness, the evolution of the radius of the precipitates slice by slice (for the seven first slices).

Some observations can be made from these results:

- The observance of the figure 3.5 enables the explanation of the general shape of the figure 3.4. At the beginning of the process, the thickening of the grain boundary is relatively fast corresponding to the onset of dissolution combined with diffusion.
  However, with the progressive disappearance of the precipitates slice by slice, this thickening becomes slower and slower. It follows a law in square root of time characterized by the straight line of the figure 3.4 (b).
  Finally, the disappearance of the particles of the last slice stops the process of growth of the grain boundary.
- The shape of the curves of the figure 3.5 are as expected. On the one hand, the order in which the precipitates vanish is logically respected with, in first the particles of the first slice (that is to say the nearest ones to the grain boundary), then the ones of the second slice, etc...
  On the other hand, the acceleration of the dissolution as the particles become smaller was predictable because of the use of the relation (3.13) for the interface velocity.
- Quantitatively, the process could seem to be very fast, but it comes from the high value of the diffusion coefficient which corresponds to diffusion of C in α-ferrite at 923 K [14].

III . 3 Second model

III . 3 . a Presentation

Compared with the model presented above, this second model accounts for the whole process of appearance and disappearance of precipitates: nucleation, growth and coarsening.

The program starts in a volume of matrix α, devoid of particles and whose average concentration in solute is directly given by the composition of the steel.
Two types of nucleation can occur: an easy nucleation which represents the situation at the grain boundary, and a more difficult one assumed as homogeneous and symbolising nucleation everywhere else. Number densities of sites are input and take into account the gap between the initial numbers of available sites in both cases ($N_H >> N_{GB}$).

III . 3 . b Working of the program

The values of $G_{\alpha\theta}$, G_α and n_θ, respectively the Gibbs energy of the system α-θ per mole of component, the Gibbs energy of α per mole of component and the number of moles of components in θ are given by MT-DATA [15]. They are necessary to obtain ΔG_v and ΔG_m, the Gibbs energy change per unit volume of embryo and per mole, respectively, entering in the calculation of nucleation rates:

$$\Delta G_m = \frac{G_{\alpha\theta} - G_\alpha}{n_\theta} f \qquad (3.18)$$

where $f=(c_b(t)-c^{\alpha\theta})/(c_b(0)-c^{\alpha\theta})$ accounts for the effect of the change in the average concentration in solute in the matrix on the Gibbs energy change. $c_b(t)$ is the mean concentration in solute in the matrix at the time t and $c_b(0)$ is the value for $t=0$.

$$\Delta G_v = \frac{\Delta G_m}{V_{mol}} \qquad (3.19)$$

where V_{mol} is the molar volume of the precipitate θ.

The consequence of the introduction of f is that, the more the mean concentration in solute in the matrix is low (because of the depletion of solute during the growth of the existing particles), the more difficult is for new embryos to nucleate.

I_H and I_{GB}, homogeneous and heterogeneous nucleation rates, are given by the relations (2.5) and (2.8) and allow to obtain the number of embryos which appear during dt:

$$\begin{aligned} \Lambda_H &= I_H \, dt \\ \Lambda_{GB} &= I_{GB} \, dt \end{aligned} \qquad (3.20)$$

Typically, the nucleation occurring at the grain boundary is so fast that all the available sites (N_{GB}) are quasi-instantaneously occupied. On the other hand, nucleation on the other sites is more spread over time and gives a large number of distributions (Λ_H, r).

During the early stages of the model, nucleation and growth occur simultaneously (Fig 3.6). The mechanism of growth of the existing particles uses the same expressions as the ones presented previously for the first model: (3.13) for the interface velocity and (3.14) for the calculation of the new radius of the particles after growth. (3.15) and (3.16) are also used but, instead of giving directly the global changes in volume and in composition, they give contributions of each distribution on them. A mere sum of these contributions allows to get the total changes. V_S in the formulae is no more the volume of a slice but the total volume of matrix.

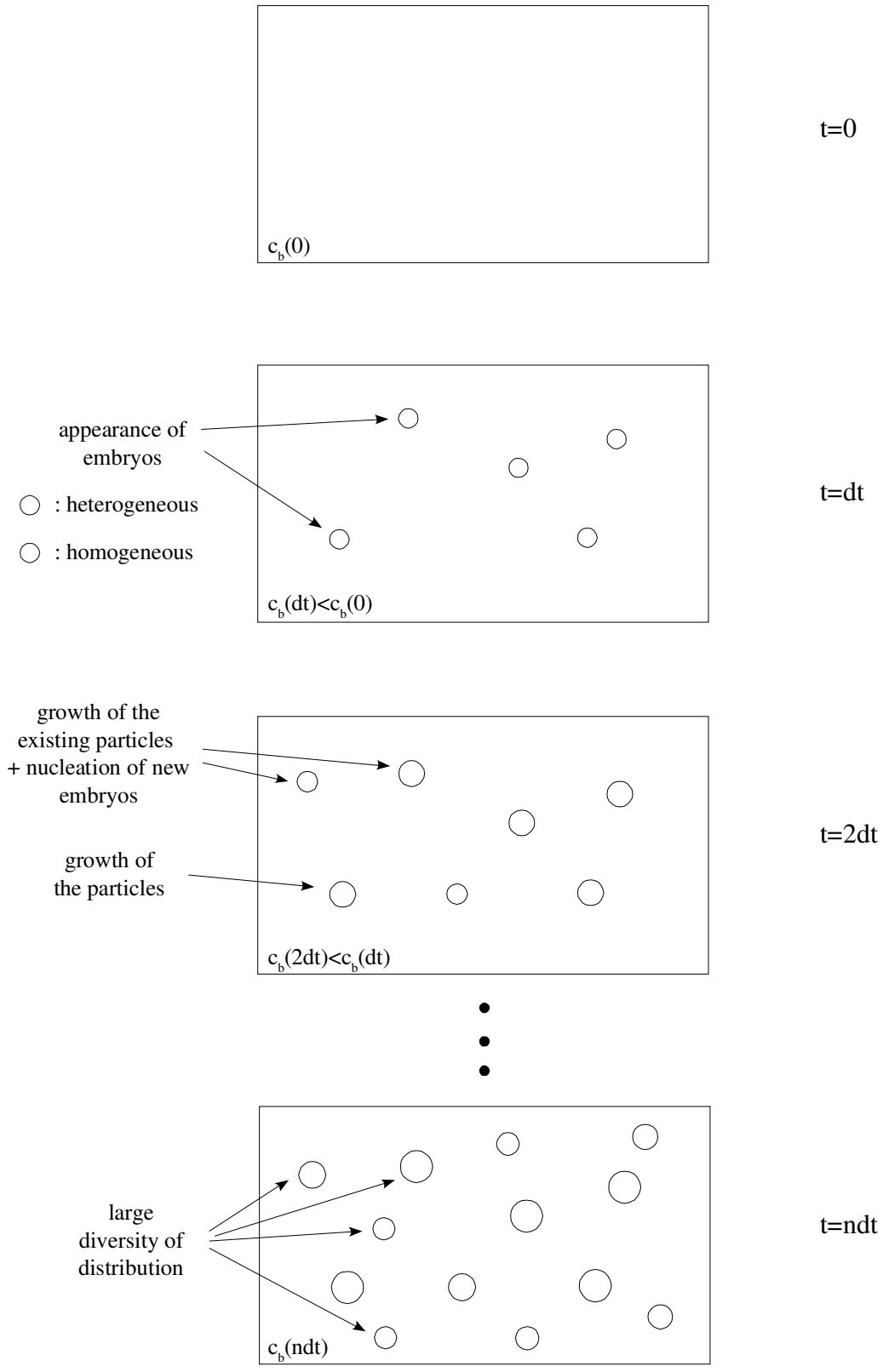

Figure 3.6: Early stages of the model (nucleation and growth).

Once nucleation is considered as negligible ($\Lambda_H < \Lambda_{Hmin}$ where Λ_{Hmin} is a value decided before the running of the program), only growth of the existing precipitates goes on.

Coarsening appears as the natural following of growth (II . 3) and uses the same expressions as for growth; only the sign changes.

III . 3 . c Results and discussion

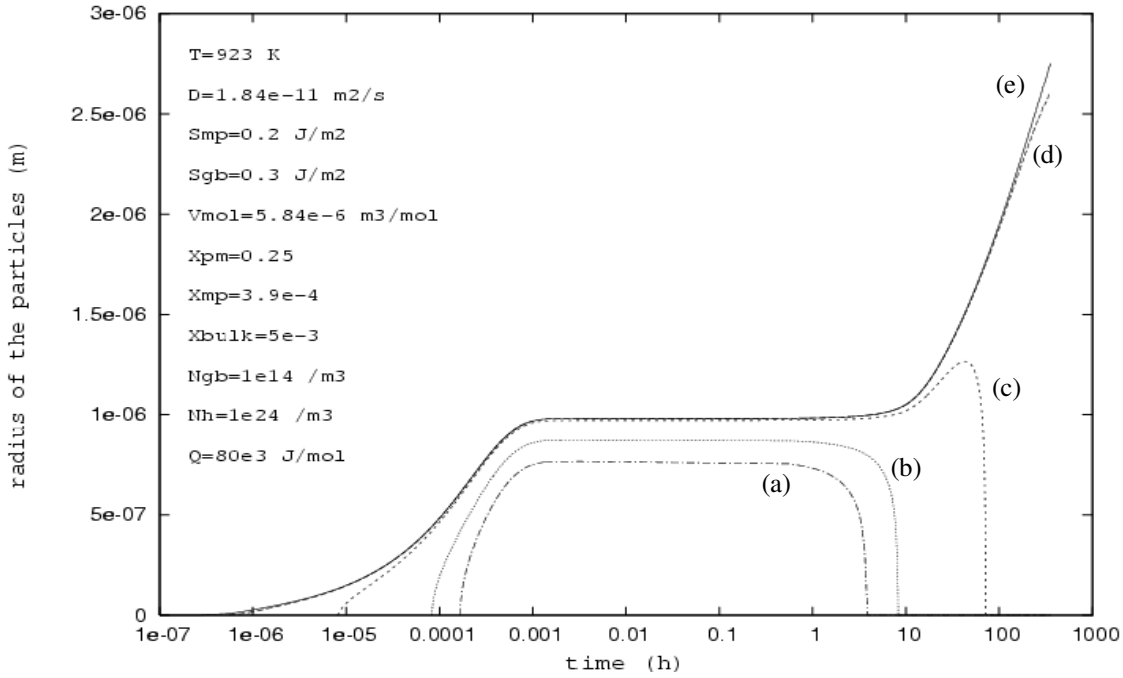

Figure 3.7: Evolution of the size of particles for some of the coexisting distributions. The continuous line represents the radius of the particles at the grain boundary.

General shape of the curves of the figure 3.7 is consistent in the sense that the three stages can be clearly identified. Nucleation is spread over time and is represented by origin of curves. Fast growth of precipitates follows that nucleation. A relatively long period of slow changes makes the link between growth and coarsening stages. It is during that period that supersaturation at the interface of the smallest particles swaps is positive sign for a negative one, so that dissolution and coarsening can start and the size of the biggest partcles can increase.

There are three kinds of curves in this diagram:

- Small particles disappear first, and this disappearance has not got a big influence on the coarsening of the other ones because of their small numbers: (a) and (b).
- Medium-size particles take advantage of dissolution of the first ones before undergo the same fate: (c) and (d).

✗ Finally, the biggest particles grow during the whole process and would stop growing after dissolution of all the other ones: (e).

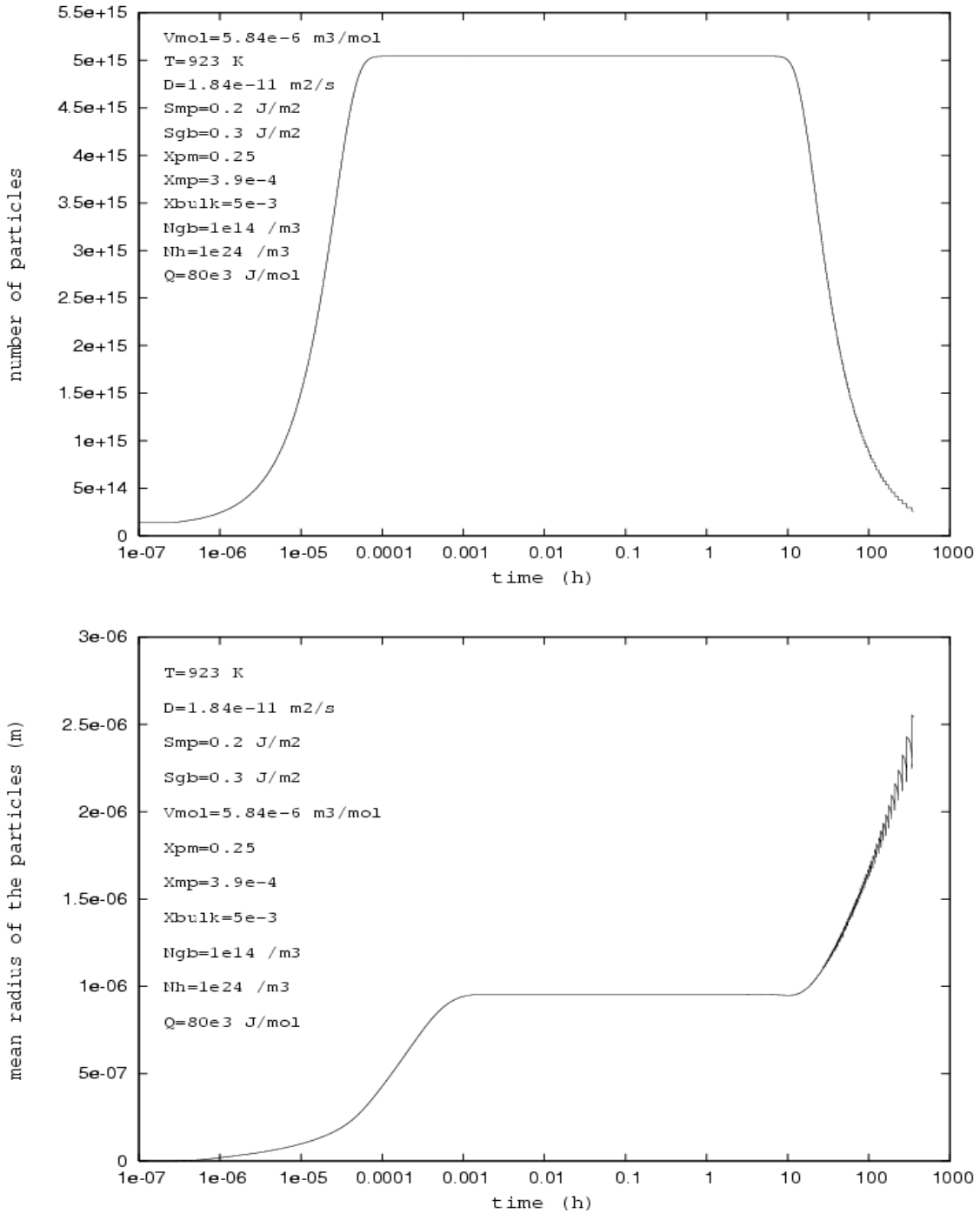

Figure 3.8: Evolution of the number (a) and mean radius (b) of particles.

Although general shape of the curves of the figure 3.8 is as expected in the eyes of the theory (2.6), some points may be discussed.

- First, the discontinuous end of the one giving the average radius of particles as a function of time is due to computation given a finite number of distributions after nucleation. An increase of this number of distributions reducts considerably the phenomenon, however, it also increase the time of computation.
- In theory, with a logarithmic scale the slope of the part representing coarsening on curve (b) should be less important than the one of the part corresponding to growth (typically, 1/2 for growth and 1/3 for coarsening). Here, this point is not respected. It reveals a defect in the model that would be linked to the calculation of the average concentration in solute after dissolution of particles. It is assumed within the model that the amount of matter lost during dissolution is uniformly redistributed in the matrix; this assumption may be too heavy even in the case of solutes with high diffusion coefficients. The resolution of this problem could be the object of future work on the topic.

CONCLUSION

As natural stores of fossil fuel runs out little by little, the necessity of saving energy becomes bigger. The improvement in efficiency of power plants comes within that necessity, besides the economic and enviromnental stakes. In this work, models dealing with nucleation, growth and coarsening of precipitates have been created. They use classical theory for phase transformation in solid state. Although they remain relatively simple since they describe mechanisms for binary systems, they provide bases for more complex approaches. The results obtained in both cases are rather consistent and lead in a good direction.

Possible future works on the models would be, for instance, to apply the model for nucleation and growth of grain bounbary precipitates first developed by Aaron and Aaronson [16] instead of considering a unique particle with an infinite radius of curvature in the first program.

In the second, it would consist on an improvement in the way to calculate the average concentration of solute in the matrix step by step.

Finally, one of the important aim would be too, to apply theory for multicomponent systems instead of binary systems in order to come closer to real behaviour of materials.

REFERENCES

[1] www.giup.com/PGS

[2] H. K. D. H. Bhadeshia: *Desing of Heat Resistant Alloys for the Energy Industries*, Proceedings of the Fifth International Charles Parsons Turbine Conference, edited by A. Strang, W. M. Banks, R. D. Conroy, G. M. McColvin, J. C. Neal & S. Simpson, Institute of Materials, Cambridge, U.K., July 2000, p. 3.

[3] P. J. Ennis and W. J. Quadakkers: *9-12% Chromium Steels: Application Limits and Potential for Further Development*, Proceedings of the Fifth International Charles Parsons Turbine Conference, edited by A. Strang, W. M. Banks, R. D. Conroy, G. M. McColvin, J. C. Neal & S. Simpson, Institute of Materials, Cambridge, U.K., July 2000, p.265.

[4] F. Abe, M. Igarashi, S. Wanikawa, M. Tabuchi, K. Kimura and K. Yamuguchi: *R & D of Advanced Ferritic Steels for 650 ˚C USC Boilers*, Proceedings of the Fifth International Charles Parsons Turbine Conference, edited by A. Strang, W. M. Banks, R. D. Conroy, G. M. McColvin, J. C. Neal & S. Simpson, Institute of Materials, Cambridge, U.K., July 2000, p.129.

[5] K. Kimura, H. Kushima, F. Abe, K. Suzuki, S. Kumai and A. Satoh: *Microstructural Change and Degradation Behaviour of 9Cr-1Mo-V-Nb Steel in the Long-Term*, Proceedings of the Fifth International Charles Parsons Turbine Conference, edited by A. Strang, W. M. Banks, R. D. Conroy, G. M. McColvin, J. C. Neal & S. Simpson, Institute of Materials, Cambridge, U.K., July 2000, p.590.

[6] J. W. Christian: *Theory of Transformations in Metals and Alloys*, Pergamond Press, Oxford, 1975.

[7] J. D. Robson and H. K. D. H. Bhadeshia: *Modelling Precipitation Sequences in Power Plant Steels*, Part 1 – Kinetic Theory, *Mater.Sci.Techn.*, 1997, p631.

[8] N. Fujita and H. K. D. H. Bhadeshia: *Modelling Simultaneous Alloy Carbide Sequence in Power Plant Steels*, *ISIJ International*, Vol. 42, No. 7, 2002, p. 760.

[9] N. Fujita and H. K. D. H. Bhadeshia: *Precipitation of Molybdenum Carbide in Steel: Multicomponent Diffusion and Multicomponent Capillarity Effects*, *Mater.Sci.Techn*, Vol. 15, June 1999, p. 627.

[10] T. Sourmail: Ph.D. Report, University of Cambridge, 2002.

[11] C. Zener: *Transactions of the American Institute of Mining and Metallurgical Engineers*, 175:15-51, 1946.

[12] M. Hilberts: *Phase Equilibria, Phase Diagrams and Phase Transformations, Their Thermodynamic Basis*, Cambridge University Press, 1998.

[13] A. Iserles: *A First Course in The Numerical Analysis of Differential Equations*, Cambridge University Press, 1996, p. 105.

[14] R. W. K. Honeycombe and H. K. D. H. Bhadeshia: *Steels Microstructure and Properties*, Second Edition, Edward Arnold, 1995, p. 7.

[15] MT-DATA: Phase Diagram Calculation Software, National Physical Laboratory, Teddington, Middlesex, U.K., 1989.

[16] H. B. Aaron and H. I. Aaronson: *Growth of Grain Bounbary Precipitates in Al-4% Cu by Interfacial Diffusion*, *Acta Metallurgica*, Vol. 16, June 1968.